Epitaxial Design of a Direct Optically Controlled GaAs/AlGaAs-Based Heterostructure Lateral Superjunction Power Device for Fast Repetitive Switching

Tirthajyoti Sarkar, *Student Member, IEEE*, and Sudip K. Mazumder, *Senior Member, IEEE*

***Abstract*—We outlined the epitaxial design methodology for a novel compound-semiconductor-based optically controlled power device for fast repetitive switching frequency. The proposed structure features gallium arsenide (GaAs/AlGaAs) lateral heterostructure with charge-balancing superjunction layers to make the breakdown voltage of the device independent of doping of the photo-absorbing GaAs active layer and linearly dependent on the lateral length. This structure also features parallel plate like p-n junction, which reduces local electric-field crowding and supports higher reverse bias during OFF-state. We show that the use of lattice-matched wider bandgap AlGaAs helps to achieve superjunction charge balancing without having any effect on switching performance of the device. We also show that the particular processing methodology (ion implantation over zinc diffusion) helps in improving the breakdown-voltage capability of the device.**

***Index Terms*—Epitaxial growth, gallium arsenide (GaAs), heterostructure, optically triggered power transistor (OTPT), power semiconductor, superjunction.**

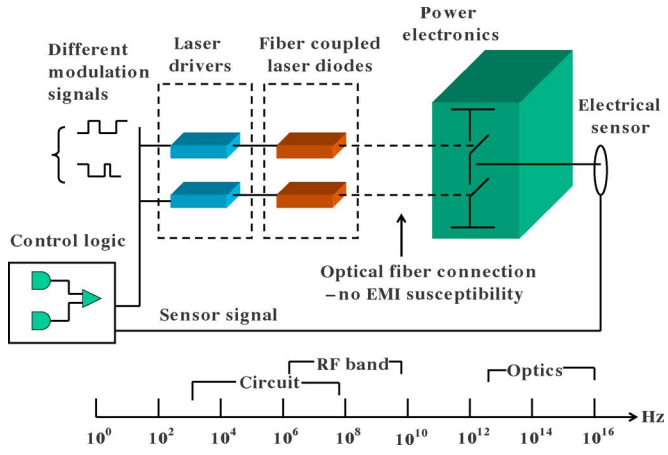

Fig. 1. Architecture of OTD-based power electronics system.

I. Introduction

In an environment where external RF signals can interact with power electronics, for example, fly-by-light architecture for next-generation avionics, electromagnetic interference (EMI) is a critical issue [1]. Recent research by U.S. Air force [2], [3] has shown that tangible reductions in weight, volume, and cost are possible through the application of emerging photonic technologies for vehicular power-management systems by elimination of EM shielding around copper wiring, which is replaced by a lightweight optical fiber. In this respect, next-generation photonic power-electronic systems, based on optically triggered devices (OTDs) [4]–[6] (as shown in Fig. 1 [6]), provide key advantages over conventional electrically triggered device (ETD)-based switching power electronics.

Direct optically controlled power device is the first major step toward photonic power-electronic systems. Most desirable properties of such a device would be: 1) high optical and electrical triggering gain; 2) nonlatched turn-on and turn-off controllabilities with a single optical monochromatic source; and 3) optical fiber coupling. Moreover, basic electrical properties like high breakdown voltage, fast switching times, and low ON-state resistance need to be met.

Optically triggered monolithic power-semiconductor devices [4], [7] include bulk photoconductive switches (PCS) [8]–[11], bistable optically controlled switches (BOSS) [12]–[15], optothyristor [16]–[18], light-triggered thyristor (LTT) [19], [20], static induction phototransistor [21]–[23], and bipolar mode field-effect transistor (BMFET) [24], [25]. It can be seen that not all of the desirable properties have been met simultaneously by these devices. For instance, LTT and optothyristors feature the inherent thyristor-like latch-up characteristic, which leads to uncontrollable and slow turn-off that is not desirable for fast repetitive switching device. BMFET exhibits long turn-on and turn-off times due to long minority carrier recombination lifetime of Si (on the order of microseconds). It is to be noted that, for direct OTDs, recombination lifetime is the key factor governing the switching speed. Similar switching speed may be exhibited by devices with varying voltage and current rating. This is in contrast to field-effect electrical power devices, where device size determines the capacitance which governs the switching speed. Therefore, a Si-based OTD can have microseconds turn-on and turn-off times in this voltage and

Manuscript received June 29, 2006. This work was supported in part by the Office of Naval Research (ONR) under Award N00014-06-1-0227 and in part by the Air Force Office of Scientific Research (AFOSR) under Award FA8650-05-M-2553. The review of this paper was arranged by Editor M. A. Shibib.

The authors are with the Laboratory for Energy and Switching-Electronics Systems (LESES), Department of Electrical and Computer Engineering, University of Illinois, Chicago, IL 60607 USA (e-mail: mazumder@ece.uic.edu).

Color versions of one or more of the figures in this paper are available online at http://ieeexplore.ieee.org.

Digital Object Identifier 10.1109/TED.2006.890231

current range. Gallium arsenide (GaAs) was chosen as the primary device material in case of PCS, BOSS, and optothyristors because of its direct bandgap nature, higher mobility, and fast photogeneration-recombination dynamics. These switches feature subnanosecond closing time, low jitter, high voltage, and current capability. For semi-insulating GaAs PCS, nonlinear gain mechanism (in the form of lock-on) has been demonstrated which minimizes the optical energy requirement for switching [10].

Conventional optically controlled power devices with vertical structure, like optothyristors or static induction transistors, generally use semi-insulating drift region [17], [18] for supporting reverse bias. This results in a large voltage drop across the device during conduction, which is not desirable in power electronics applications from efficiency point of view. ETDs like power MOSFETs or IGBTs use controllably low-doped voltage sustaining layer to keep a balance between blocking voltage capability and ON-state resistance. An OTD, which uses base conductivity modulation principle like IGBT, will have no problem from low-doped layer resistance. But, such a device will exhibit slow switching due to additional time required for conductivity modulation (during turn-on) and minority carrier recombination in a low-doped background (during turn-off). This is a trade-off between device gain, forward drop, and switching speed, and for low-frequency applications, such a device would be useful. But in this paper, as we are focusing on high-frequency applications, conductivity modulation is not employed, and therefore, semi-insulating voltage blocking layer is not a good option.

Growing thick ($> 15-20\ \mu$m) controllably doped GaAs epitaxial layer poses yield and reliability problems using common growth methods. This is because most of the research, development, and commercialization in traditional GaAs-based switching devices fall in the category of high-speed MESFET, optoelectronic switches and ICs, RF and microwave devices including HBT, HEMT, HFET, etc., where thin lateral epitaxial structure has been the dominant form. For achieving high blocking voltage in such a structure, superjunction concept [32], [33] can be applied, although currently, there is no known compound-semiconductor-based superjunction power device.

We recognize an advantage of adopting lateral structure for superjunction GaAs power device from fabrication point of view. Being a delicate material from thermal point of view, GaAs fabrication demands as low a thermal budget as possible. Fabrication of the vertical superjunction structure requires multiple epitaxy growth and implantation, with subsequent high-temperature drive-in process [32]–[34] which increases the total thermal budget manifold. Instead, a lateral superjunction structure can be fabricated by single epitaxial growth and low-temperature diffusion process, and hence, such a lateral device is more reliable and easier to fabricate in GaAs technology.

Moreover, in the lateral optically triggered power transistor (OTPT) [5], [6] structure (illustrated in Fig. 2), we can obtain almost vertical p-body region by diffusion or implantation to create parallel-plate p-n junction, which is theoretically best junction profile to support reverse bias [26].

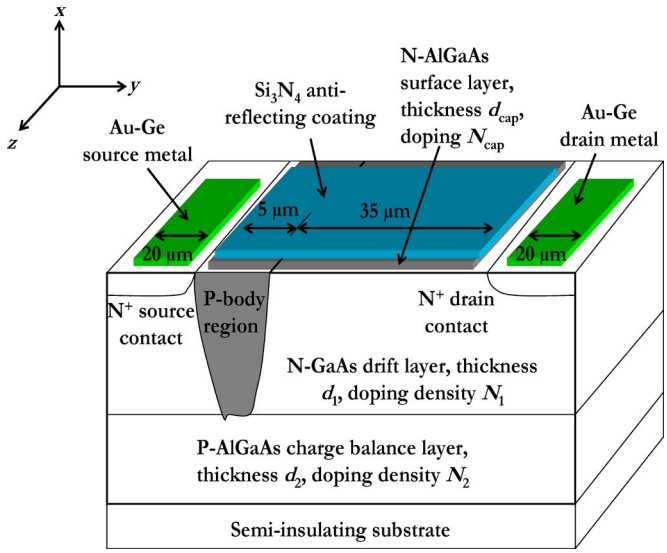

Fig. 2. Schematics of the OTPT structure (not drawn to the scale).

Furthermore, lattice-matched AlGaAs can be used as the charge-compensating layer in the superjunction structure. Due to the wider bandgap of AlGaAs than GaAs, no photogeneration occurs in that region and, as such, the design and optimization of this layer does not interfere with the device switching performance. We note that unlike HBT or HFET, heterojunction in the OTPT is not being used to improve electron mobility or high-frequency response. Purpose of using AlGaAs is to reduce the design complexity of the epitaxial structure by decoupling the mechanisms of photogeneration (during conducting phase) and superjunction charge balancing (during nonconducting phase).

The prospective applications for such a lateral fast switching optically controlled power device include power management systems in military and commercial aircrafts, spacecrafts, electric warships, naval planes and helicopters, battle tanks, armored cars, and field artillery vehicles. In short, any military or commercial automotive electric power management system, which may be affected by intentional or unintentional RF/EMI signal, has the need of such device for enhanced survivability. Moreover, as can be seen from Fig. 1, such device is triggered directly by light and therefore does not need a voltage reference or a voltage differential between source and gate like most widely used power devices, i.e., MOSFET or IGBT. This simplifies the driver circuit by eliminating the need to have separate high-side (whose voltage reference is at a much higher voltage above ground) and low-side drivers (voltage reference at ground) for multilevel power circuit topology. The advantage of complete electrical isolation between driver and power stage, coupled with the aforementioned driver simplicity, extends the possible application areas of device into: 1) flexible ac transmission systems, 2) active power filters, 3) motor drives, 4) telecommunication, and 5) distributed generation.

This paper focuses on AlGaAs/GaAs heteroepitaxial superjunction concept and the epitaxial design method for OTPT. Sensitivity of the device breakdown voltage on the imbalance in the charge content of the epitaxial layers has been investigated

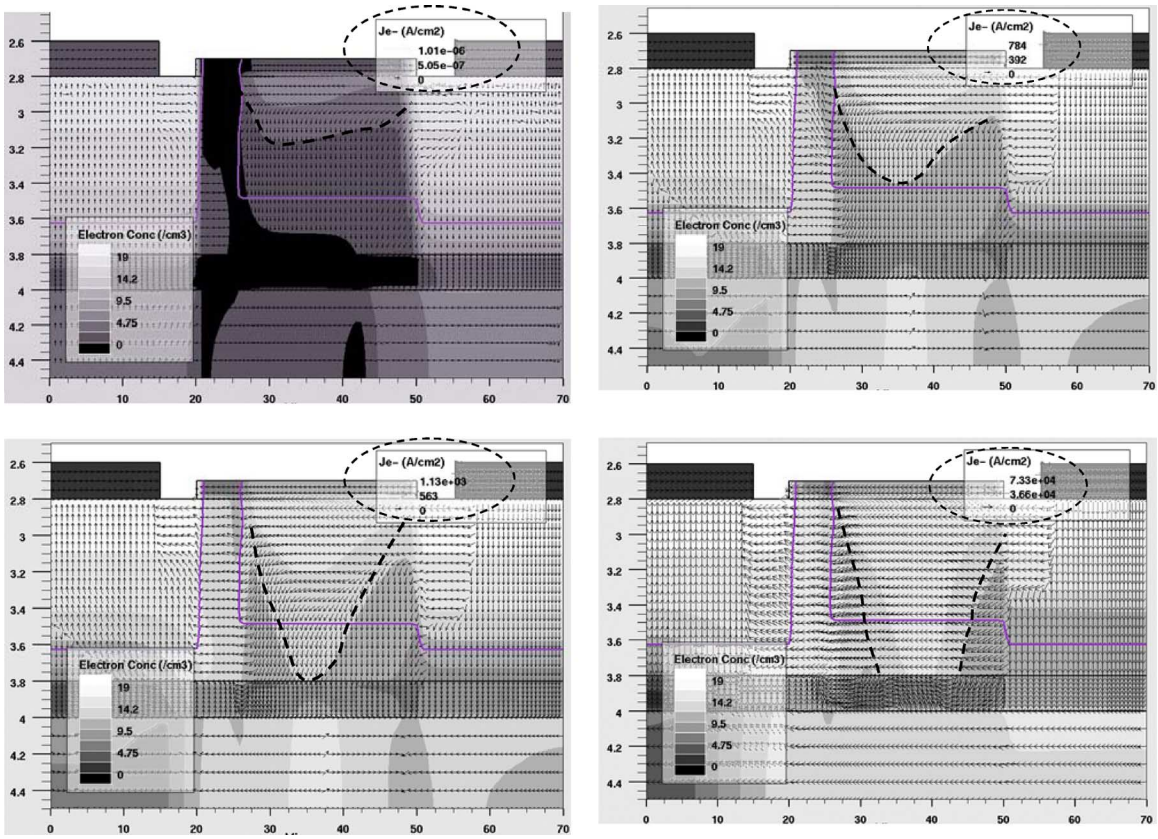

Fig. 3. Gradual increment in electron concentration from transient # 1 to transient # 4 inside OTPT when optical beam triggers the device. Each transient is separated by a 2-ns time interval. The high-concentration area is marked by a dotted line and can be seen to be increasing in depth with time progression. Also, the electron current density figures are marked by a dotted ellipse.

in detail. It has been shown that the common trade-off problem between breakdown-voltage sensitivity and ON-state resistance for superjunction power MOSFETs is not exhibited by OTPT. Sensitivities for separate processing sequence have been compared. Moreover, sensitivity studies for different thicknesses of the GaAs layer have been carried out because the optical triggering efficiency depends on this thickness which is also intrinsically linked up with superjunction sensitivity. This gives the designer a choice to trade off between charge-balance sensitivity and optical triggering efficiency.

II. Epitaxial Design of the OTPT

A. Device Structure and Operation

We have shown in Fig. 2 the structural schematic of the OTPT reported earlier in [5] and [6]. It has a lateral structure with two electrodes—source and drain. Shallow low-energy implanted N^+ regions make the contacts between these electrodes and the semiconductor. The bottom p-type AlGaAs layer acts as the charge-compensating layer, and a thin AlGaAs surface barrier layer is there on top of GaAs n-drift layer. The optical window is defined by the 100-nm-thick Si_3N_4 antireflecting layer between the electrodes. This particular thickness results in minimum reflection of light from the front surface of the device. The doping and thickness values of the epitaxial layers d_1, d_2, N_1, N_2, $d_{\rm cap}$, and $N_{\rm cap}$ have been designed such as to realize the superjunction charge balance, i.e., the total positive charge contributed by p-AlGaAs layer nullifies the total negative charge contributed by the top n-type layers.

The OTPT structure features a deep-implanted p-body which extends all the way up to the p-AlGaAs layer. The junction between the p-body and the n-drift region results in almost ideal parallel plate like electric-field distribution during the blocking state. This p-body region does not have any metal gate and is electrically floating. Therefore, no gate capacitance is present, and the possibility of dv/dt induced spurious turn-on of the device (unintentional charging of gate capacitance through high dv/dt across the drain–source terminal in case of a power MOSFET switching transient) is reduced.

A wider bandgap AlGaAs surface barrier layer is used to suppress Fermi-pinning and surface recombination velocity effects [27]–[29], which may degrade the overall device performance by lowering the optical triggering efficiency significantly and increasing the ON-resistance. As this surface, AlGaAs layer is transparent to the operating wavelength; no light is absorbed here. Effectively, the conducting channel is formed little below the surface (buried channel), and no performance degradation occurs due to surface defects. Switching performance of the OTPT is hardly affected due to the absence of photogeneration in this region.

In the blocking or open state, the applied voltage is supported by the reverse-biased p-n junction between the p-body and n-drift regions. When triggering light beam falls on the device,

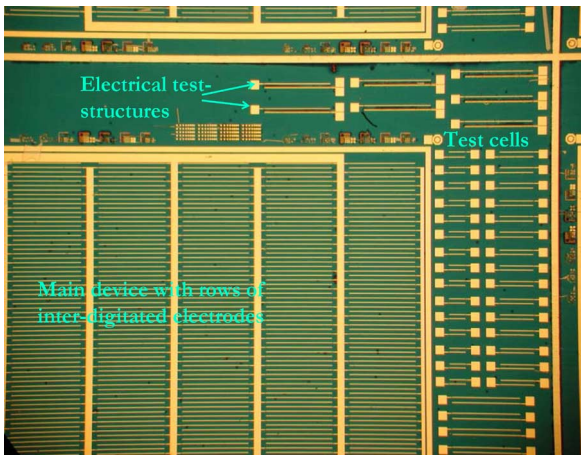

Fig. 4. Photomicrograph of the OTPT device prototype.

in the optical window region, it is absorbed and it generates electron-hole plasma by photogeneration. They are mobilized by the local electric field and are attracted by the drain and source electrodes, and constitute electron and hole currents thereby closing the switch (shown in Fig. 3). If the light beam is sustained, the conductivity is sustained too and the switch remains closed. When the light shuts OFF, the carriers are recombined among themselves and the switch goes back to its high-resistivity blocking state. The device gain (defined as the ratio between the drain–current and photogenerated current) and the switching speed of the OTPT depend strongly on the minority carrier recombination lifetime. A shorter lifetime ensures a faster turn-off due to rapid recombination when the light shuts OFF, but it also leads to low device gain. A design trade-off is necessary depending upon particular application. Minority carrier lifetime can be influenced by increasing the doping concentration in the p-body region, thereby enhancing nonradiative recombination rate [37].

Figs. 4 and 5 show the micrographs of a prototype OTPT device. These devices have 1.0-μm-thick n-GaAs (doping density $\sim 5.0 \times 10^{13}$ cm^{-3}) layer grown [by metalo-organic chemical vapor deposition (MOCVD) technique] on top of 300-nm-thick $P-Al_{0.2}Ga_{0.8}As$ layer (doping density of 3.0×10^{14} cm^{-3}). A 100-nm n-AlGaAs layer (doping density 1.45×10^{15} cm^{-3}) is grown and patterned for surface passivation. Si implantation at 100-keV energy with 5.0×10^{14} cm^{-2} dose is carried out for N^+ source and drain contact regions. Beryllium implantation at 150 keV and 2.0×10^{13} cm^{-2} dose has been used to create the p-body. Activation of both n- and p-type implants is carried out at a rapid thermal processor at 850 °C for 5 min using a GaAs undoped wafer as proximity anneal cap. Plasma-enhanced chemical vapor deposited Si_3N_4 of 100-nm thickness is used as antireflective (AR) coating. p-type guard rings are created around individual test structures for reducing electric fields on the edge. Electron beam evaporated Au-Ge alloy (annealed at 400 °C) is used as drain and source contacts, and thick Cr-Au metallization is done to form bonding pads. This is the first ever experimental prototype of compound-semiconductor-based heterostructure superjunction high-voltage power device for switching power electronics applications.

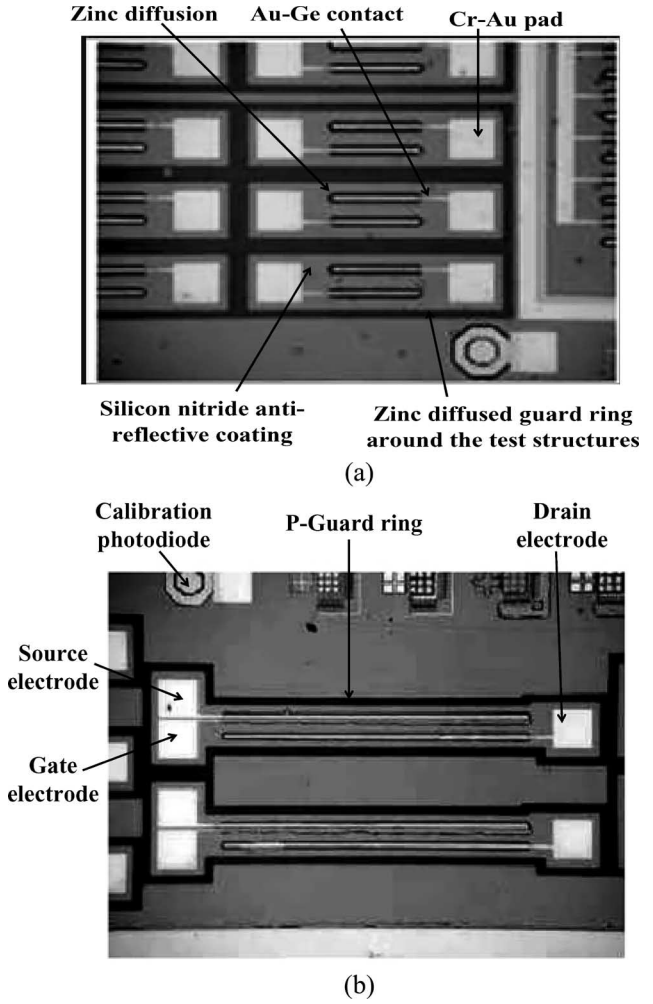

Fig. 5. Micrograph of OTPT showing (a) zinc diffused region, metallization, and AR coating, and (b) calibration photodiode and electrical three-terminal test structure.

TABLE I
DEVICE PARAMETERS FOR SIMULATION OF OTPT

N-GaAs layer thickness	2.0 μm	N-AlGaAs layer thickness	0.1 μm
N-GaAs layer doping	5.0×10^{14} cm^{-3}	N-AlGaAs layer doping	1.0×10^{15} cm^{-3}
P-AlGaAs layer thickness	1.1 μm	P-body peak doping	1.0×10^{18} cm^{-3}
P-AlGaAs layer doping	1.0×10^{15} cm^{-3}	N-source and drain doping	1.0×10^{19} cm^{-3}

B. Epitaxial Design Rule

For charge compensation, the total charges of the n-GaAs drift layer (Q_N) and p-AlGaAs layer (Q_P) need to be considered. This yields

$$\begin{aligned} Q_N = Q_P &\Rightarrow z(L_{\text{drift}} + x_{\text{drain}})d_1 N_{\text{drift}} \\ &= z(L_{\text{drift}} + x_{\text{drain}})d_2 N_{\text{CC}} \Rightarrow d_1 N_{\text{drift}} \\ &= d_2 N_{\text{CC}} \end{aligned} \quad (1)$$

where z is the width of the OTPT. However, we observed that due to relatively small values of d_1 and d_2, $(\sim 1-2\ \mu\text{m})$ the total charge balance gets affected by the charge contribution

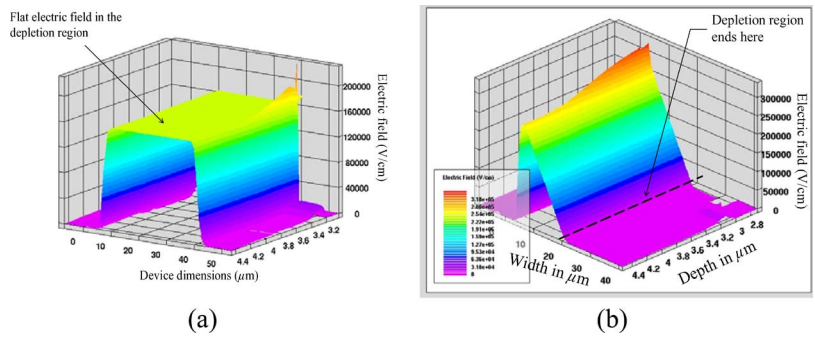

Fig. 6. Two-dimensional electric-field profiles for (a) superjunction and (b) nonsuperjunction structures.

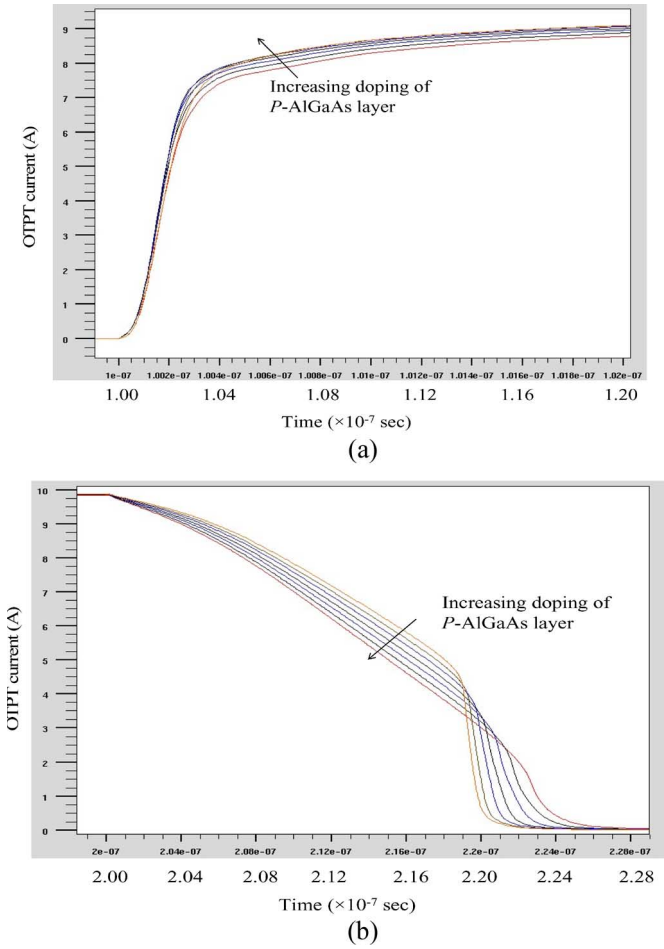

Fig. 7. Impact of p-AlGaAs layer doping and thickness variation on (a) rise and (b) fall time of OTPT.

from the thin-surface AlGaAs barrier layer as well. Thus, (1) modifies to

$$d_1 N_{\text{drift}} + d_{\text{cap}} N_{\text{cap}} = d_2 N_{\text{CC}} \tag{2}$$

where the surface barrier layer has been assumed to be n-type (the polarity does not affect the surface passivation property). This is because typical doping density values indicate that making this layer p-type requires extremely low thickness (< 1000 Å) or uncharacteristically low doping level ($< 1.0 \times 10^{15}$ cm^{-3}); both of which are unsatisfactory from a processing standpoint.

TABLE II
OPTICAL AND ELECTRICAL PARAMETERS FOR MIXED DEVICE-CIRCUIT SIMULATION

Bias voltage	400 V	Optical wavelength	808 nm
Load resistance	40 Ω	Switching frequency	1 MHz
Optical power density	200 W/cm^2	Laser rise & fall time	2.5 ns

When exactly charge-compensated, i.e., $Q_n = -Q_p$, in the drift region, the Poisson's equation can be written as

$$\begin{aligned} \frac{dE}{dx} &= -\frac{Q}{\varepsilon_r \varepsilon_o} \Rightarrow \frac{dE}{dx} \\ &= -\frac{(Q_n + Q_p)}{\varepsilon_r \varepsilon_o} \Rightarrow \frac{dE}{dx} \\ &= 0 \Rightarrow E \\ &= \text{constant}. \end{aligned} \tag{3}$$

The constant value can be given by the gradient of the voltage applied across source and drain terminals, i.e.,

$$E = \frac{V}{L_{\text{drift}}}. \tag{4}$$

C. Breakdown Voltage and ON-State Resistance

For OTPT, 1-D drift-diffusion equations were coupled with a photogeneration mechanism to estimate basic quantities like ON-state resistance, breakdown voltage, etc. Breakdown voltage can be estimated from the impact ionization model of GaAs [38]

$$\begin{aligned} \int_0^{L_{\text{drift}}} &\left[2.994 \times 10^5 \exp\left(-(6.648 \times 10^5 L_{\text{drift}}/V_{\text{Br}})^{1.6}\right)\right. \\ &\left. + 2.215 \times 10^5 \exp\left(-(6.57 \times 10^5 L_{\text{drift}}/V_{\text{Br}})^{1.75}\right)\right] dx \\ &= 1. \end{aligned} \tag{5}$$

For estimation of ON-state resistance, we need to obtain a steady-state carrier concentration by solving continuity equation. We assume that both Shockley–Read–Hall (SRH) and radiative band-to-band direct recombination occur in OTPT

because of the direct bandgap nature of GaAs. The photogeneration rate is given by

$$G_n(y) = G_p(y) = \eta(1-R)\frac{P\lambda}{hc}\alpha e^{-\alpha y} = G(y). \quad (6)$$

The SRH recombination rate for electron and holes is given by [26] v

$$R_{\mathrm{SRH},n} = \frac{n}{\tau_a} \quad R_{\mathrm{SRH},p} = \frac{p}{\tau_a}. \quad (7)$$

The radiative recombination rate is the same for electrons and holes and is given by [26]

$$R_{\mathrm{rad}} = C_d\left(pn - n_i^2\right). \quad (8)$$

For steady–state 1-D case, assuming constant mobility, and that electric field is almost constant, we obtain the second-order ordinary differential equations governing the electron and hole concentrations as

$$D_a\frac{d^2n}{dx^2} + \mu_a E\frac{dn}{dx} - \left(\frac{1}{\tau_a} + C_d p\right)n = -\left[G_n(y) + C_d n_i^2\right] \quad (9\text{-a})$$

$$D_a\frac{d^2p}{dx^2} + \mu_a E\frac{dp}{dx} - \left(\frac{1}{\tau_a} + C_d n\right)p = -\left[G_n(y) + C_d n_i^2\right]. \quad (9\text{-b})$$

For calculating the ON-state resistance of OTPT, we recognize the two main components as p-body resistance and n-drift resistance and write the overall ON-state resistance as

$$R_{\mathrm{on}} = R_{\mathrm{body}} + R_{\mathrm{drift}} = \frac{L_{\mathrm{body}}}{\int_0^d q\left(n(x)+p(x)\right)\mu_{a,\mathrm{body}} Z dy} + \frac{L_{\mathrm{drift}}}{\int_0^d q\left(n(x)+p(x)\right)\mu_{a,\mathrm{drift}} Z dy}. \quad (10)$$

Using (7) and (8), we can write down the R_{on} in the compact form

$$R_{\mathrm{on}} = \frac{\sum_{\substack{j=1,2\\k=1,2}} L_j\left(\left(\frac{1}{D_j\tau_j}+\frac{C_jN_{j,k}}{D_j}\right)\sqrt{\left(\frac{\mu_j}{D_j}E\right)^2+4\left(\frac{1}{D_j\tau_j}+\frac{C_jN_{j,k}}{D_j}\right)}\right)}{qZ\sum_{\substack{j=1,2\\k=1,2}}\int_0^{d_1}\left[G(y)+C_jn_i^2\right](K_1m_{2,j,k}-K_2m_{1,j,k})\mu_j dy}. \quad (11)$$

In (9), $\mu_1 = \mu_{a,\mathrm{body}}$, $\mu_2 = \mu_{a,\mathrm{drift}}$, $D_1 = D_{a,\mathrm{body}}$, $D_2 = D_{a,\mathrm{drift}}$, $\tau_1 = \tau_{a,\mathrm{body}}$, $\tau_2 = \tau_{a,\mathrm{drift}}$, and the different doping concentrations are given by, $N_{1,1} = N_{\mathrm{body}}$, $N_{1,2} = n_i^2/N_{\mathrm{body}}$, $N_{2,1} = N_{\mathrm{drift}}$, $N_{2,2} = n_i^2/N_{\mathrm{drift}}$. Also, K_1 and K_2 are two constants to be determined from boundary conditions and so are dependent on specific geometry and doping definition of the device and

$$m_{1,j,k} = \frac{-\left(\frac{\mu_j}{D_j}E\right)+\sqrt{\left(\frac{\mu_j}{D_j}E\right)^2+4\left(\frac{1+\tau_jC_dN_{j,k}}{D_j\tau_j}\right)}}{2}$$

$$m_{2,j,k} = \frac{-\left(\frac{\mu_j}{D_j}E\right)-\sqrt{\left(\frac{\mu_j}{D_j}E\right)^2+4\left(\frac{1+\tau_jC_dN_{j,k}}{D_j\tau_j}\right)}}{2}. \quad (12)$$

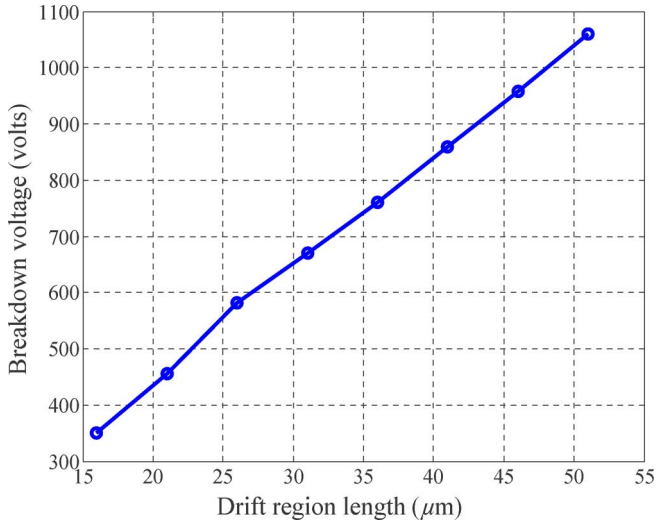

Fig. 8. Linearity between breakdown voltage and drift region length when charge balance is satisfied.

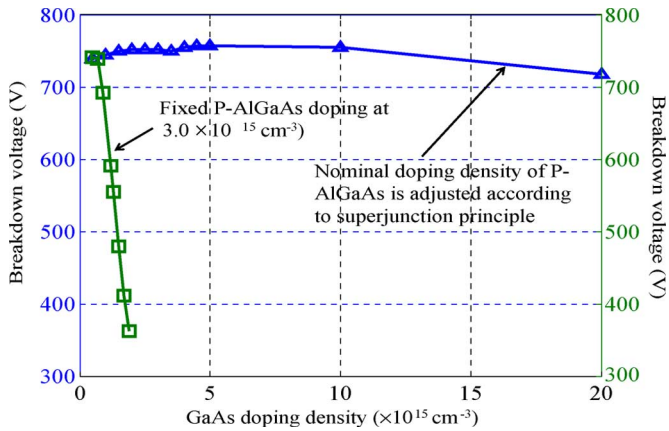

Fig. 9. Superjunction principle ensures high breakdown voltage even though the GaAs doping density varies over a wide range.

III. Superjunction Sensitivity Studies

We present sensitivity study results in four parts. First, we show the operation of a basic superjunction structure and the usefulness of superjunction concept in maintaining the breakdown voltage at high value even if the doping densities of individual layers vary over wide range. Second, we present superjunction sensitivity results for different sheet charge densities (defined later) and show that unlike electrically triggered superjunction MOSFETs, OTPT exhibits no trade-off between breakdown-voltage sensitivity and ON-state resistance. Next,

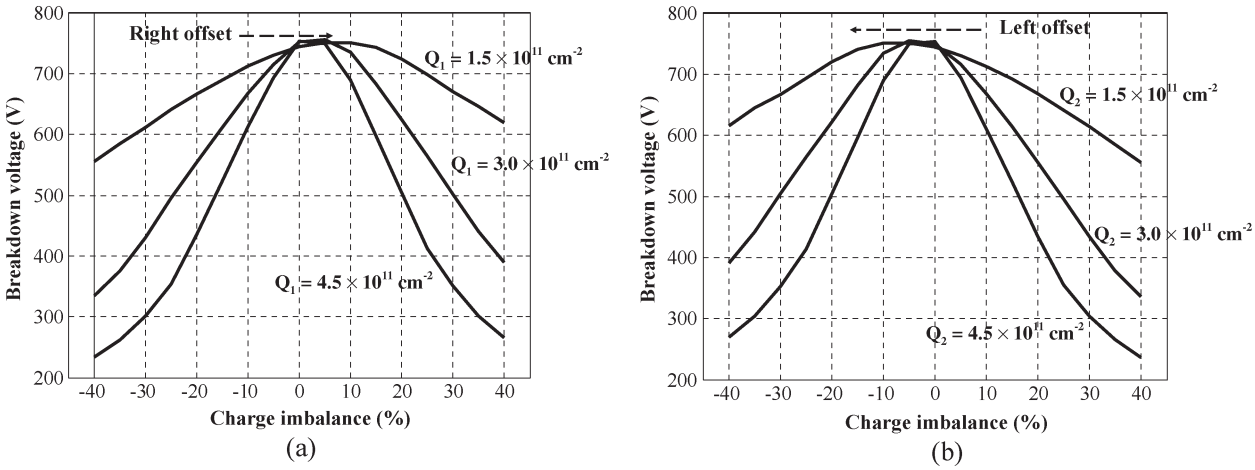

Fig. 10. Breakdown-voltage sensitivity with (a) p-AlGaAs and (b) GaAs doping density variations for different sheet charge densities.

we show how this sensitivity depends on processing method by simulation and experimental validation. Finally, we show how the sensitivity depends on GaAs layer thickness and establish that, unlike electrically triggered superjunction device, in OTPT, the sensitivity is intrinsically linked with a triggering efficiency.

A. Linearity of Breakdown Voltage With Respect to Drift Length and Independence of GaAs Doping Density

Table I shows the key parameters, calculated according to (2), for a representative device structure. Fig. 6 shows the comparison between breakdown electric-field distribution inside the device for superjunction and nonsuperjunction structure. Suitably designing the doping level and the thickness of different epitaxial layers ensures charge balance such that the entire drift region is depleted of mobile carriers in the OFF-state and the resulting electric field is constant. The important difference from conventional RESURF lateral power devices is that for OTPT, there is no metal gate electrode and thus no spreading of depletion region from the n-drift-p-AlGaAs junction toward the surface, as described, a primary feature of lateral RESURF devices in [39]. Therefore, the electric field is more or less constant in the vertical direction throughout the drift region in a perfectly charge-compensated structure.

We show that p-AlGaAs layer does not interfere with the switching performance of OTPT. Marginal variations (in the order of few nanoseconds) can be seen from the switching simulations in Fig. 7(a) and (b) when the doping of this layer is varied from 1.0×10^{15} to 1.0×10^{16} cm^{-3} while maintaining the superjunction condition by changing the thickness. Simulation parameters for the resistive load circuit are listed in Table II.

When the charge-balance condition is satisfied, we obtain $L_{\rm drift} \sim L_{\rm depletion}$, and the breakdown voltage $V_{\rm Br}$ of the device can be approximated as follows:

$$V_{\rm Br} \approx E_c L_{\rm depletion} = E_c L_{\rm drift} \tag{13}$$

where E_c denotes the critical breakdown field for GaAs and $L_{\rm depletion}$ denotes the depletion width of the p-n junction between the p-body and n-drift region. Therefore, the breakdown voltage is expected to be linearly dependent on the length of the drift region. In Fig. 8, it is shown that the breakdown voltage of OTPT is linearly dependent on the drift length when the charge-balance condition is satisfied.

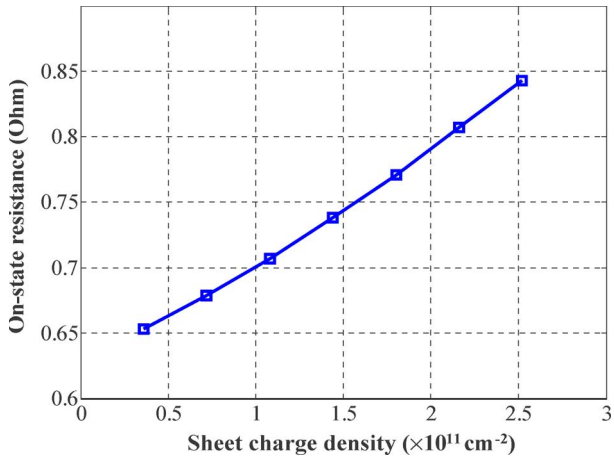

Fig. 11. ON-state resistance variation with sheet charge density. This characteristic is opposite to that exhibited by conventional electrically triggered superjunction power devices for example CoolMOS.

The utility of superjunction charge balancing can be comprehended from Fig. 9 which shows that for a nonsuperjunction structure, the breakdown voltage of the OTPT drops rapidly with an increasing GaAs doping density, whereas for a superjunction structure, by varying the p-AlGaAs doping density, the breakdown voltage can be kept at almost the same level over a wide range of doping densities. This is because for nonsuperjunction structures, the depletion width is determined by the lower doped side, i.e., n-drift region doping density (N_1). Higher doping density results in shorter depletion width and lower breakdown voltage. But for the superjunction structure, the breakdown voltage is almost independent of the drift doping because of fixed depletion width.

B. Superjunction Charge-Balance Sensitivity and ON-State Resistance for Different Sheet Charge Densities

Because of background contaminations, epitaxial growth cannot guarantee an exact charge balance as required by (2).

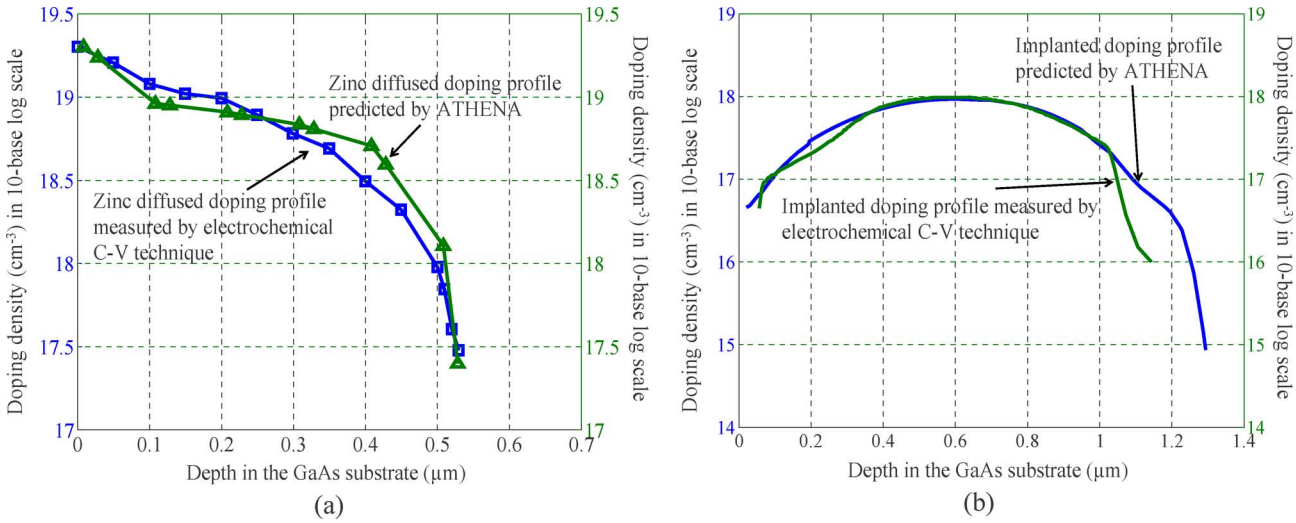

Fig. 12. Experimental validation of the process modeling of (a) zinc diffusion and (b) beryllium implantation.

It is therefore necessary to estimate how much the breakdown voltage varies with mutual charge imbalance (CI) between different layers. We conducted sensitivity studies for different sheet charge densities. Similar studies on superjunction vertical power MOSFETs have been reported in [34]–[36] specifically with respect to CoolMOS device. We show that unlike vertical superjunction MOSFETs, the trade-off problem between superjunction sensitivity and ON-state resistance, present in, is nonexistent in OTPT. We define sheet charge density, in line with [34], as the product of epitaxial layer thickness and doping density, i.e., $Q_1 = d_1 N_1$ for the GaAs layer and $Q_2 = d_2 N_2$ for the p-AlGaAs layer. Fig. 10 shows the sensitivity of the breakdown voltage due to variation in p-AlGaAs and GaAs doping density for different Q-values. CI has been defined as: $\%\mathrm{CI} = (N_{\mathrm{actual}} - N_{\mathrm{nominal}})/N_{\mathrm{nominal}}$, where N_{nominal} denotes the doping density to achieve charge balance and N_{actual} denotes the value of true doping density.

We note that the sensitivity curves are not entirely symmetric with respect to the origin. This implies that the design rule of (2) is not exactly valid for OTPT structure. This attributed to the addition of extra charge from the p-body region to the total p-type charge density. Because of this, a slightly lower p-AlGaAs epitaxial doping density or slightly higher n-GaAs doping density than predicted by (2) would give a peak breakdown voltage. Consequently, curves in Fig. 8(a) are slightly right offset and the curves of Fig. 8(b) are slightly left offset. We can therefore modify (2) as

$$d_1 N_1 + d_{\mathrm{cap}} N_{\mathrm{cap}} = d_2 N_2 + \int_0^{d_1} N_{\mathrm{body}}(y)\,dy \qquad (14)$$

where $N_{\mathrm{body}}(y)$ denotes the vertical dopant-density profile.

We observe from Fig. 10 that lower sheet charge density results in lesser sensitivity of breakdown voltage to CI. This is also true in the case of vertical superjunction power MOSFETs. However, lower Q entails higher ON-state resistance for superjunction MOSFET [31], whereas it results in slightly lower

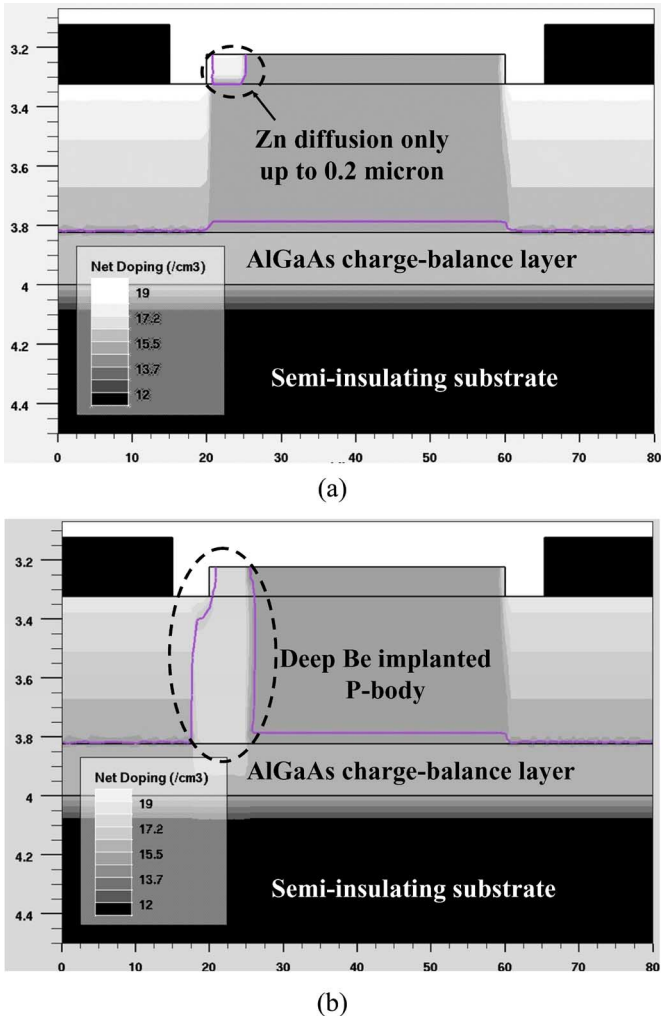

Fig. 13. OTPT device modeled with (a) 850-°C 5-min Zn diffusion, and (b) 100-keV $4 \times 10^{13}-\mathrm{cm}^{-2}$ dosage beryllium implant followed by 850-°C 5-min thermal activation.

ON-state resistance in OTPT. This is due to less degree of recombination of photogenerated carriers for a lower background charge density and follows from (11). For the same $G(y)$ and

TABLE III
NOMINAL EPITAXIAL PARAMETERS FOR OTPT MODEL

GaAs thickness	0.5 μm	GaAs doping	5.0×10^{-14} cm^{-3}
P-AlGaAs thickness	0.177 μm	P-AlGaAs doping	3.1×10^{15} cm^{-3}
N-AlGaAs thickness	0.1 μm	N-AlGaAs doping	3×10^{15} cm^{-3}

thickness d_1, lowering N_{drift} would lower R_{on}. Fig. 11 shows the variation of ON-state resistance with different Q-values (obtained by varying N_{drift} but keeping d_1 fixed) for OTPT for the same optical power. The switching simulation was done using a resistive load circuit with bias voltage of 100 V across OTPT in series with a 10-Ω resistance. The optical power density for switching was 200 W/cm^2, and the wavelength was 808 nm.

C. Dependence of Superjunction Charge-Balance Sensitivity on Processing Methodology

During process validation, we observed that for reasonable temperature (< 850 °C) and time of diffusion (5 min), open-tube spin-on zinc diffusion method results in a dopant concentration that falls rapidly after $\sim$0.5 μm. Fig. 12(a) shows the experimentally calibrated data (obtained using electrochemical C–V profiling by a polaron) and the simulated doping profile. This shallow diffusion depth does not reach up to the bottom p-AlGaAs layer which is illustrated in Fig. 13(a) for an OTPT device with 0.5-μm-thick GaAs layer. In a CI condition, there is a chance of current leakage if the p-body does not guard the N^+ source from the drift region and this may lead to lower breakdown voltage. To solve this shallow diffusion depth problem, we conjectured that an ion implantation, which ensures a p-type column all the way up to the p-AlGaAs layer, would improve the superjunction sensitivity to CI. Consequently, we modeled an OTPT device [shown in Fig. 13(b)] by a process simulation using 100-keV beryllium implantation with 4×10^{13} cm^{-2} dosage, followed by 5-min 850-°C thermal activation. Fig. 12(b) shows the experimental validation of the implanted doping profile predicted by a process simulation.

We conducted three different sensitivity studies on OTPT devices with both zinc diffused and beryllium implanted p-body. Parameters for the device model are given in Table III. The nominal doping densities for the charge-balance condition have been taken from the calibrated data of MOCVD epitaxial-growth process.

The breakdown-voltage sensitivity results are shown in Figs. 14–16, respectively. We observe that the change in the processing technique results in the improvement in breakdown voltages for the same degree of CI caused by doping density variations in n-AlGaAs and n-GaAs layers. However, the doping density variation in p-AlGaAs layer affects the OTPT device with an implanted p-body in almost the same way as it does for the OTPT with zinc diffused p-body.

Fig. 17(a) and (b) shows the experimental breakdown characteristics for the OTPT. The implanted device shows higher breakdown voltage and lower leakage current as predicted by a numerical simulation. Both devices have the exact same processing sequence except for p-body formation, and use identical mask set. Both characterizations were done using Tektronix 371A high-power curve tracer and Signatone probe station.

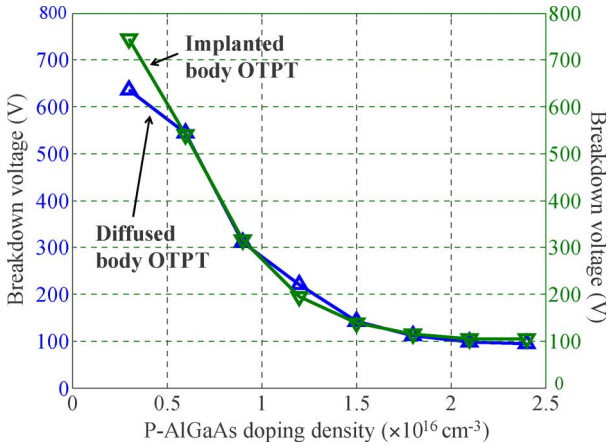

Fig. 14. Comparative breakdown-voltage variation with varying p-AlGaAs doping density for zinc diffused and beryllium implanted structures.

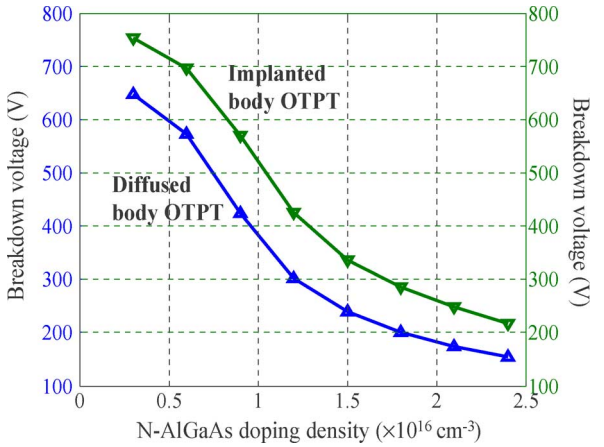

Fig. 15. Comparative breakdown-voltage variation with varying n-AlGaAs surface layer doping density for zinc diffused and beryllium implanted structures.

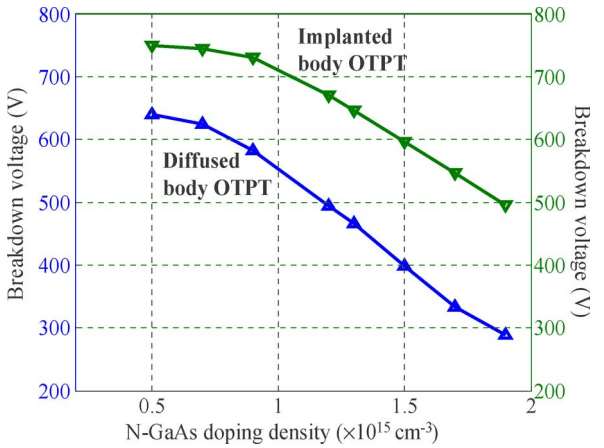

Fig. 16. Comparative breakdown-voltage variation with varying n-GaAs layer doping density for zinc diffused and beryllium implanted structures.

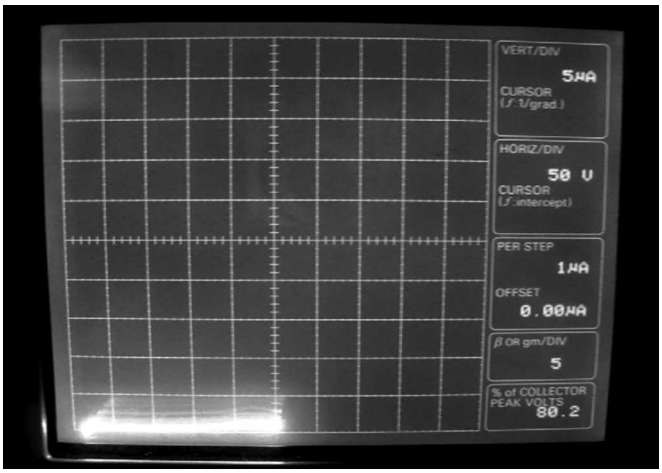

(a)

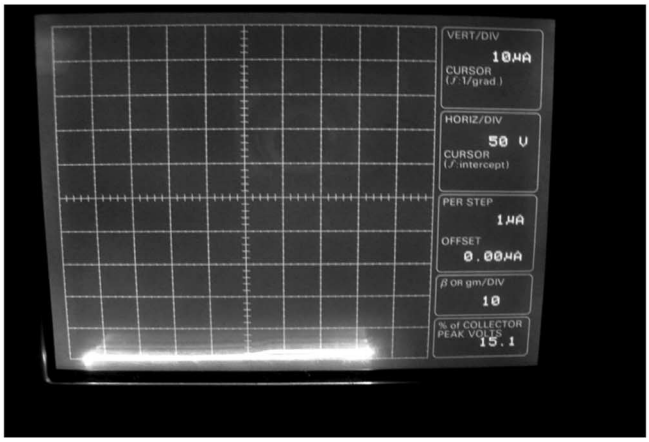

(b)

Fig. 17. Experimental validation of the improved breakdown voltage of OTPT with implanted body over zinc-diffused body. (a) 250 V with zinc-diffused body (voltage scale of 50 V/div, current scale of 5 μA/div), (b) 430-V, $\sim 2-\mu$A leakage with Be-implanted body, (voltage scale of 50 V/div, current scale of 10 μA/div).

D. Superjunction Charge-Balance Sensitivity for Different Thicknesses of Photoactive GaAs Layer

From a switching power device point of view, a thicker GaAs layer is desirable because it results in a higher photogeneration due to higher amount of optical absorption and entails lower ON-state resistance. This also follows from (11) where increasing d_1 lowers $R_{\rm on}$. Fig. 18 shows that OTPT with 0.5-μm-thick GaAs exhibits too high ON-state resistance because a significant portion of incident light remains unabsorbed. This is because the absorption depth in GaAs for 808-nm wavelength light is > 1 μm [30], [31]. As this GaAs thickness d_1 is intrinsically linked up in the superjunction charge-balance condition [as in (2) or (4)], its variation may cause a different degree of superjunction sensitivity. This mutual coupling of superjunction sensitivity and triggering efficiency is a unique feature for optically triggered superjunction devices like OTPT.

Figs. 19–21 show the variation in breakdown voltage with variation in p-AlGaAs, n-AlGaAs, and GaAs layer doping for four different GaAs layer thicknesses. We observe that for

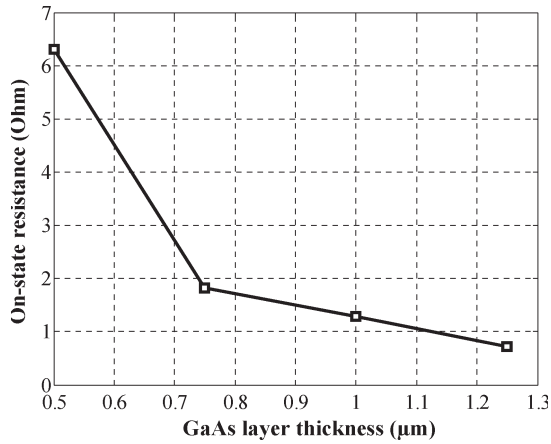

Fig. 18. ON-state resistance versus GaAs layer thickness for the same optical triggering power.

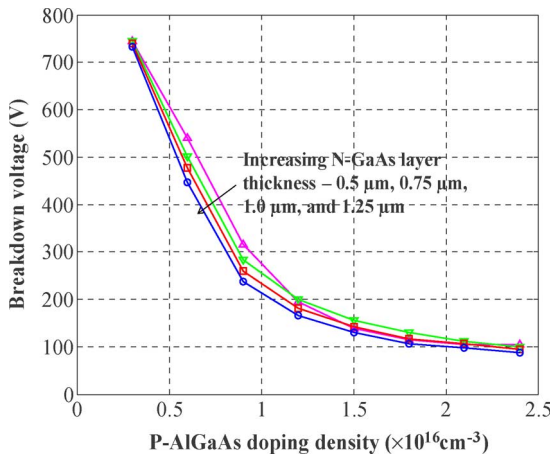

Fig. 19. Breakdown-voltage variation with p-AlGaAs doping density for four different GaAs thicknesses.

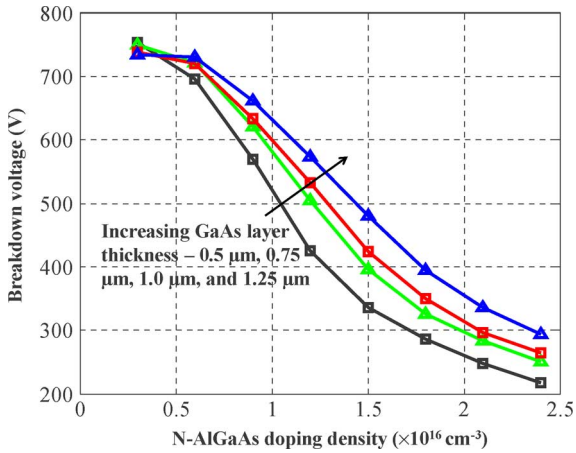

Fig. 20. Breakdown-voltage variation with n-AlGaAs doping density for four different GaAs thicknesses.

variation in p-AlGaAs and n-GaAs layer doping densities, the breakdown-voltage variation becomes more pronounced for thicker GaAs layer. In the case of n-AlGaAs surface layer doping variation, the sensitivity decreases for thicker GaAs layer.

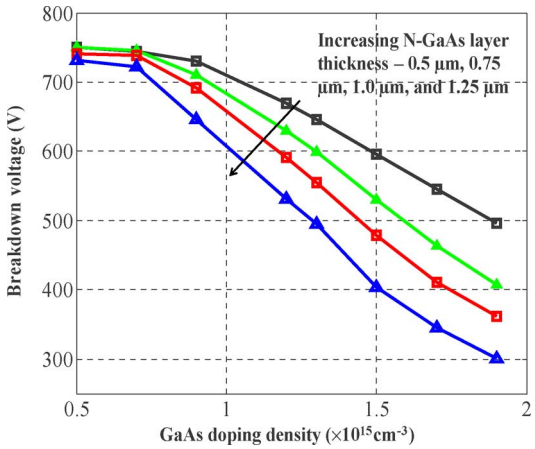

Fig. 21. Breakdown-voltage variation with n-GaAs doping density for four different GaAs thicknesses.

IV. Conclusion

We demonstrate that a GaAs/AlGaAs-based superjunction lateral heterostructure solves the simultaneous problems of achieving high breakdown voltage and fast repetitive switching frequency in an optically triggered power device without requiring thick GaAs low-doped substrate. Lateral structure offers the simplicity of controlled epitaxial growth to realize charge-balanced superjunction structure. The choice of AlGaAs layer for the superjunction (instead of GaAs) precludes carrier generation in that region due to its wider bandgap than GaAs, thereby enabling the optimal realization of epitaxial-growth parameters for high breakdown electric field without affecting turn-on and turn-off times.

A simple design rule relating epitaxial layer thickness and doping density can be formulated based upon the charge-balance condition. This must also include the charge contribution from body region. Diversion from superjunction charge-balance condition results in lower breakdown voltage. Unlike electrically triggered superjunction power MOSFETs (e.g., CoolMOS), in case of OTPT, lower sheet charge density helps achieve both less sensitivity and low ON-state resistance.

Ion implantation may substitute zinc diffusion method for ensuring that the vertical p-type column extends up to the bottom p-AlGaAs layer. This reduces the sensitivity of the breakdown-voltage variation for CI caused by the doping density variation in n-AlGaAs and n-GaAs layers. However, it does not affect the sensitivity caused by p-AlGaAs layer CI. Therefore, for the best design, p-AlGaAs layer doping density and growth rate need to be controlled with maximum accuracy.

When GaAs layer thickness is increased, superjunction sensitivity increases for CI caused by variation in the doping densities of p-AlGaAs and GaAs layers but decreases for n-AlGaAs layer induced CI. Therefore, designing OTPT with higher GaAs layer thickness for lower ON-state resistance and higher optical triggering efficiency needs stricter control on doping density, particularly for p-AlGaAs and n-GaAs layers during epitaxial-growth process.

Acknowledgment

The authors would like to thank Dr. A. Sugg for the tasks related to the OTPT processing. Any opinions, findings, conclusions, or recommendations expressed herein are those of the authors and do not necessarily reflect the views of the ONR or AFOSR.

Patent disclaimer: The work described in this paper, including the sections and the figures therein, are protected by the following patent application filed by the University of Illinois at Chicago: S. K. Mazumder and T. Sarkar, "Optically triggered power system and devices," USPTO PCT/US2006/024839, filed on June 23, 2006. Original provisional patent application filed CY083 filed in September 2005.

References

[1] J. J. Ely, G. L. Fuller, and T. W. Shaver, "Ultrawideband electromagnetic interference to aircraft radios," in *Proc. Digital Avionics Syst. Conf.*, 2002, vol. 2, pp. 13E4-1–13E4-12.

[2] J. R. Todd, "Direct optical control: A lightweight backup consideration," in *Proc. IEEE Nat. Aerosp. and Electron. Conf.*, 1992, vol. 2, pp. 456–463.

[3] [Online]. Available: http://www.afrlhorizons.com/Briefs/Apr05/VA0412.html

[4] S. K. Mazumder, T. Sarkar, M. Dutta, and M. S. Mazzola, "Photoconductive devices in power electronics," in *Electrical Engineering Handbook*, 3rd ed. New York: Taylor & Francis, 2005, pp. 9.43–9.59. invited book chapter.

[5] S. K. Mazumder and T. Sarkar, "Device technologies for photonically-switched power-electronic systems," in *Proc. IEEE Int. Pulsed Power Conf.*, 2005.

[6] ——, "Optically-triggered power transistor (OTPT) for fly-by-light (FBL)/EMI susceptible power electronics," in *Proc. IEEE Power Electron. Spec. Conf.*, Jun. 18–22, 2006, pp. 1–8. Plenary Paper.

[7] A. Rosen and F. Zutavern, *High-Power Optically Activated Solid-State Switches*. Boston, MA: Artech House, 1994.

[8] F. Lacassie, D. Kaplan, Th. De Saxce, and P. Pignolet, "Two photon absorption in semi-insulating gallium arsenide photoconductive switch irradiated by a picosecond infrared laser," *Eur. Phys. J., Appl. Phys.*, vol. 11, no. 3, pp. 189–195, 2000.

[9] S. Wei, Z. Xian-Bin, L. Qi, C. Er-Zhu, and Z. Wei, "High gain lateral semi-insulating GaAs photoconductive switch triggered by 1064 nm laser pulses," *Chin. Phys. Lett.*, vol. 19, no. 3, pp. 351–354, Mar. 2000.

[10] F. J. Zutavern, G. M. Loubriel, H. P. Hjalmarson, A. Mar, W. D. Helgeson, M. W. O'Malley, M. H. Ruebush, and R. A. Falk, "Properties of high gain GaAs switches for pulsed power applications," in *Proc. 11th IEEE Int. Pulsed Power Conf.*, 1997, vol. 2, pp. 959–964.

[11] M. Buttram, "Some future directions for repetitive pulsed power," in *Proc. Pulsed Power Plasma Sci.*, 2001, vol. 1, pp. 3–8.

[12] M. S. Mazzola, K. H. Schoenbach, V. K. Lakdawala, and S. T. Ko, "Nanosecond optical quenching of photoconductivity in a bulk GaAs switch," *Appl. Phys. Lett.*, vol. 55, no. 20, pp. 2102–2104, Nov. 1989.

[13] D. C. Stoudt, R. A. Roush, M. S. Mazzola, and S. F. Griffiths, "Investigation of a laser-controlled, copper-doped GaAs closing and opening switch for pulsed power applications," in *Proc. 8th IEEE Pulsed Power Conf.*, 1991, pp. 41–44.

[14] D. C. Stoudt, R. P. Brinkmann, R. A. Roush, M. S. Mazzola, F. J. Zutavern, and G. M. Loubriel, "Subnanosecond high-power performance of a bistable optically controlled GaAs switch," in *Proc. 9th IEEE Pulsed Power Conf.*, 1993, pp. 72–75.

[15] F. E. Peterkin, K. H. Schoenbach, R. Dougal, and J. Hudgins, "Developments toward laser diode driven bistable photoconductive switches (BOSS)," in *Proc. 10th IEEE Int. Pulsed Power Conf.*, 1995, vol. 1, pp. 366–371.

[16] J. H. Hur, P. Hadizad, S. R. Hummel, P. D. Dapkus, H. R. Fetterman, and M. A. Gundersen, "GaAs opto-thyristor for pulsed power applications," in *Proc. 19th IEEE Power Modulator Symp.*, 1990, pp. 325–329.

[17] J. H. Zhao, T. Burke, D. Larson, M. Weiner, A. Chin, J. M. Ballingal, and T. H. Yu, "Sensitive optical gating of reverse-biased AlGaAs/GaAs optothyristors for pulsed power switching applications," *IEEE Trans. Electron Device*, vol. 40, no. 4, pp. 817–823, Apr. 1993.

[18] R. J. Lis, J. H. Zhao, L. D. Zhu, J. Illan, S. McAfee, T. Burke, M. Weiner, W. R. Buchwald, and K. A. Jones, "An LPE grown InP based optothyristor for power switching applications," *IEEE Trans. Electron Devices*, vol. 41, no. 5, pp. 809–813, May 1994.
[19] T. Nimura, Y. Tsunoda, Y. Tadokoro, and N. Yamano, "A 8 kV 3500 A light triggered thyristor," in *Proc. 7th Int. Symp. Power Semicond. Devices and ICs*, 1995, pp. 181–184.
[20] J.-L. Sanchez, R. Berriane, J. Jalade, and J. P. Laur, "Functional integration of MOS and thyristor devices: A useful concept to create new light triggered integrated switches for power conversion," in *Proc. 5th Eur. Conf. Power Electron. and Appl.*, 1993, vol. 2, pp. 5–9.
[21] K. I. Nuttall and W. Chen, "Numerical simulation study of a novel 400 V static induction phototransistor," *Semicond. Sci. Technol.*, vol. 11, no. 3, pp. 443–454, Mar. 1996.
[22] P. Hadizad, J. H. Hur, H. Zhao, K. Kaviani, M. A. Gundersen, and H. R. Fetterman, "A high-voltage optoelectronic GaAs static induction transistor," *IEEE Electron Device Lett.*, vol. 14, no. 4, pp. 190–192, Apr. 1993.
[23] P. Hadizad, J. H. Hur, H. Zhao, J. Osinski, P. D. Dapkus, M. A. Gundersen, and H. R. Fetterman, "GaAs optoelectronic static induction transistor for high frequency pulsed power switching," in *Proc. 8th IEEE Int. Pulsed Power Conf.*, 1991, pp. 200–203.
[24] G. Breglio, R. Casavola, A. Cutolo, and P. Spirito, "The bipolar mode field effect transistor (BMFET) as an optically controlled switch: Numerical and experimental results," *IEEE Trans. Power Electron.*, vol. 11, no. 6, pp. 755–767, Nov. 1996.
[25] G. Vitale, G. Busatto, and G. Ferla, "The switching behavior of the bipolar mode field effect transistor (BMFET)," in *Proc. IEEE Ind. Appl. Soc. Annu. Meeting*, 1988, vol. 1, pp. 600–605.
[26] B. J. Baliga, *Power Semiconductor Devices*. Boston, MA: PWS-Kent, 1996.
[27] S. Tiwari, *Compound Semiconductor Device Physics*. New York: Academic, 1991.
[28] W. S. Lee, D. Ueda, T. Ma, Y. C. Fao, and J. S. Harris, "Effect of emitter-base spacing on the current gain of AlGaAs/GaAs hetero-junction bipolar transistor," *IEEE Electron Device Lett.*, vol. 10, no. 5, pp. 200–202, May 1989.
[29] O. Nakajima, K. Nagata, H. Ito, T. Ishibashi, and T. Sugeta, "Suppression of emitter size effect on current gain in AlGaAs/GaAs HBTs," *Jpn. J. Appl. Phys.*, vol. 24, no. 10, pp. 1368–1369, Oct. 1985.
[30] J. Pastriiak, F. Karel, and O. Petiieek, "Optical absorption coefficient of semiconductors in the extrinsic region obtained by photoconductivity measurements: Application to SI GaAs," *J. Semicond. Sci. Technol.*, vol. 5, no. 8, pp. 867–870, Aug. 1990.
[31] M. Brozel and G. Stillman, Eds., *Properties of Gallium Arsenide*, London, U.K.: Inst. Electr. Eng., 1986.
[32] D. Shahrjerdi, B. Hekmatshoar, A. Khakifirooz, and M. Fathipour, "An approach to low-cost fabrication of lateral COOLMOS structures," in *Proc. Int. Semicond. Device Res. Symp.*, 2003, pp. 272–273.
[33] T. Minato, T. Nitta, A. Uenisi, M. Yano, M. Harada, and S. Hine, "Which is cooler, trench or multi-epitaxy? Cutting edge approach for the silicon limit by the super trench power MOS-FET (STM)," in *Proc. 12th Int. Symp. Power Semicond. Devices and ICs*, 2000, pp. 73–76.
[34] P. M. Shenoy, A. Bhalla, and G. M. Dolny, "Analysis of the effect of charge imbalance on the static and dynamic characteristics of the super junction MOSFET," in *Proc. 11th Int. Symp. Power Semicond. Devices and ICs*, 1999, pp. 99–102.
[35] H. Zhong, Y. C. Liang, G. S. Samudra, and X. Yang, "Practical superjunction MOSFET device performance under given process thermal cycles," *Semicond. Sci. Technol.*, vol. 19, no. 8, pp. 987–996, Aug. 2004.
[36] L. Lorenz, G. Deboy, A. Knapp, and M. Marz, "COOLMOS—A new milestone in high voltage power MOS," in *Proc. 11th Int. Symp. Power Semicond. Devices and ICs*, 1999, pp. 3–10.
[37] G. B. Lush, H. F. MacMillan, B. M. Keyes, D. H. Levi, M. R. Melloch, R. K. Ahrenkiel, and M. S. Lundstrom, "A study of minority carrier lifetime versus doping concentration in n-type GaAs grown by metalorganic chemical vapor deposition," *J. Appl. Phys.*, vol. 72, no. 4, pp. 1436–1442, Aug. 1992.
[38] G. E. Bulman, V. M. Robbins, K. F. Brennan, K. Hess, and G. E. Stillman, "Experimental determination of impact ionization coefficients in (100) GaAs," *IEEE Electron Device Lett.*, vol. EDL-4, no. 6, pp. 181–185, Jun. 1983.
[39] Z. Parpia and C. A. T. Salama, "Optimization of RESURF LDMOS transistors: An analytical approach," *IEEE Trans. Electron Devices*, vol. 37, no. 3, pp. 789–796, Mar. 1990.

Tirthajyoti Sarkar (S'03) received the Bachelor of Technology degree (with President's Silver Medal honor) in instrumentation engineering from Indian Institute of Technology, Kharagpur, India, in 2003. Currently, he is working toward the Ph.D. degree in the area of optically triggered power-semiconductor devices.

In 2003, he joined the Laboratory for Energy and Switching-electronics Systems, Department of Electrical and Computer Engineering, University of Illinois, Chicago. His research interests are in semiconductor devices modeling, simulation, process modeling, integrated circuits, and power electronics. He has published four international conference papers and has coauthored a book chapter on optically triggered power devices.

Sudip K. Mazumder (SM'03) received the Ph.D. degree from the Department of Electrical and Computer Engineering, Virginia Polytechnic Institute and State University, Blacksburg, in 2001.

He is the Director of the Laboratory for Energy and Switching Electronics Systems and an Associate Professor with the Department of Electrical and Computer Engineering, University of Illinois, Chicago. He has more than ten years of professional experience and has held R&D and design positions in leading industrial organizations. He has published more than 60 refereed and invited journals and conference papers. His current areas of interests are interactive power electronics/power networks, renewable and alternate energy systems, and new device and systems-on-chip enabled higher power density.

Dr. Mazumder is the Editor-in-Chief of the *International Journal of Power Management Electronics*. He is also an Associate Editor of the IEEE TRANSACTIONS ON INDUSTRIAL ELECTRONICS and was the Associate Editor of the IEEE POWER ELECTRONICS LETTERS until 2005. He is a Reviewer for six international journals. He was a recipient of the Diamond Award from the University of Illinois for his outstanding research performance in 2006; the Office of Naval Research Young Investigator Award, the National Science Foundation CAREER Award, and the Department of Energy Solid State Energy Conversion Alliance Award in 2005, 2003, and 2002, respectively; and the Prize Paper Award from the IEEE TRANSACTIONS ON POWER ELECTRONICS and the IEEE Power Electronics Society in 2002.